Towards Passively Actuated Short-Range Telehaptics for Astronauts

Matvey Boguslavskiy
Dyson School of Design Engineering, Imperial College London, UK

Digby Chappell
Harvard John A. Paulson School of Engineering and Applied Sciences, Harvard University, Cambridge, MA, USA

Thrishantha Nanayakkara
Dyson School of Design Engineering, Imperial College London, UK

Abstract

Human extra-vehicular activity (EVA) plays a vital role in current and near future space exploration for two reasons: the superior dexterity exhibited by human astronauts, and their flexible problem-solving and decision-making capabilities. However, the dexterity of astronauts during EVA is limited by the flexibility and tactility of their EVA suit gloves, which are primarily designed to provide thermal insulation and pressure for the hand. This creates a compromise between utility and protection. To address this compromise, a Passively Actuated Short-range Telehaptic (PAST) device is proposed. The PAST device couples the motion of fingers between a robotic hand and a human hand through a hydraulically actuated linkage. It also transfers tactile information, including pressure, direction of motion, and position of contact, via a taxel array. Results demonstrate that the proposed prototype PAST device surpasses an unpressurised benchmark heavy work glove (HWG) in tasks involving tactile position and motion direction identification. This provides evidence supporting the feasibility of enhancing astronaut dexterity during EVA through the use of PAST devices as an alternative paradigm to gloves.

2012 ACM Subject Classification Hardware → Haptic devices; Computer systems organization → Robotic control; Human-centered computing → Haptic devices; Hardware → Sensor devices and platforms

Keywords and phrases Extra-vehicular Activity, Mechanism Design, Haptics, Dexterity, Tactility

Digital Object Identifier 10.4230/OASIcs.SpaceCHI.2025.21

Acknowledgements This project would not have been possible without the generous support, equipment and advice of the REDS and MORPH labs at the Dyson School of Design Engineering at Imperial College London. Thanks also go to Theodore Macklin of the Mechanical Engineering department at Imperial College for his insights on the history of spacesuit design.

1 Introduction

Extra-vehicular Activity (EVA) by humans is a vital aspect of past, current, and near-future space exploration endeavours. EVA allows for crucial maintenance, repair, and scientific fieldwork, enabling safer and more ambitious missions in the challenging environment of space. Productive work during EVA has historically been limited to a maximum of 8 hours, primarily due to partial-pressure exposure constraints and human endurance limitations [12]. Various potential hazards to human health and life during EVA include, but are not limited to, extreme contact surface temperatures ($\approx -150°C$ to $150°C$), heightened radiation doses, chemical contamination, and micrometeoroids [12]. In protecting astronauts from these hazards, EVA suits dramatically impair dexterity, leading to a severe limitation on the number and complexity of EVA tasks that can be completed. The existing design requirements for EVA gloves have resulted in a compromise between protection and utility, a design

approach that has remained largely unchanged since the 1970s [11]. Despite efforts, due to the inherent compromise between protection and utility, current gas-pressurised glove designs offer dexterity "[comparable] to that of heavy work gloves" [12] and remain the most common source of injuries among astronauts during spacewalks [1].

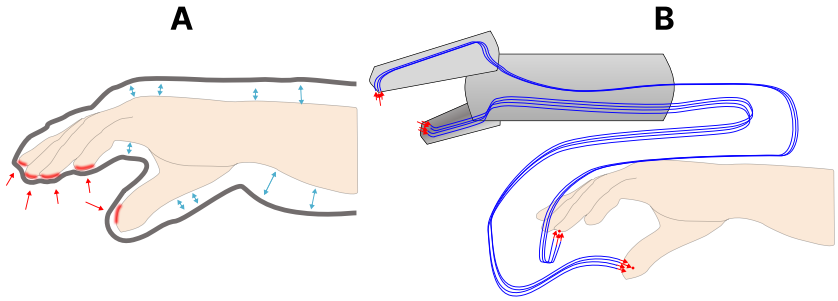

Figure 1 Image **A** illustrates the causes of loss of flexibility and tactility in conventional EVA gloves from thick insulation and the pressurised volume of the glove. The insulation diffuses precise points of pressure through the fabric. Image **B** illustrates the connection between the fingertips of the astronaut and the robotic hand via hydraulic channels that transfer tactile information to multiple points on each finger.

During EVA, astronauts engage in various tasks that require the manipulation of objects using tools or their own gloves. However, the stiffness of the gloves resulting from internal pressurization has significantly hampered hand dexterity [19] and contributed to hand injuries [1]. To enable improved dexterous manipulation, it is crucial to avoid inhibiting the astronaut's somatosensory system through high resistive forces or signal-diffusing insulation [16]. One proposed approach to deal with this degradation of dexterity from EVA gloves is an active stiffness-compensating exo-skeleton [15]. This decreases forces that the fingers of the astronauts repeatedly experience and may reduce injuries and improve dexterity through minimising fatigue. However, this solution would not significantly enhance tactility, while also creating potential injury-causing failure modes. A promising approach to improve flexibility and tactility of space suits is to apply mechanical counter-pressure (MCP) to the body rather than atmospheric pressure [17]. This would improve dexterity by increasing flexibility of the hands and reducing fatigue, by removing the 'air spring' for the fingers to work against. However, the requirements of insulative protection of the hands would still hinder tactility. MCP is at an early technology readiness level, despite being first proposed in the 1950s [10]. Currently, MCP systems struggle to achieve uniform pressure distribution, especially on concave sections of the body, and fail to ensure the same thermal contact insulation as incumbent solutions.

Certain mission-critical tasks can be accomplished remotely by leveraging telepresence (TP) [7], eliminating direct personnel risk by creating a layer of separation between the operator and potential hazards. This approach is used terrestrially for handling hazardous materials, such as radioactive samples, biohazards, and explosive devices. It can also be used with specialised tools such as in surgical TP robots to maximise performance of specific tasks [18]. However, TP may bring significant drawbacks with distance induced latency and lower mission flexibility [14]. Actuation and sensing limitations creating lack of responsiveness lead to a loss of dexterity. To address these drawbacks, short range solutions are favoured for minimising latency and information loss. Passively actuated or directly driven systems are favoured for responsiveness and minimising complexity.

Hydraulic-based passively actuated haptic systems are well suited to EVA. Hydraulic tele-haptic systems have been demonstrated for other applications, with the human-safe haptic TP robot providing a human user with precise force and position control of a humanoid *bibrachial* robot with instant feedback [21]. Hydraulic actuation as a paradigm for local teleoperation is becoming more attractive due to its possibility to be designed into high transparency mechanisms, providing high fidelity force feedback [6]. Passive sensory transfer has also been demonstrated through an air-mediated interface in application to arm prostheses, in order to transfer pressure from a robotic hand to the forearm of the user [2]. This approach is suitable for low fidelity signal feedback due to the compressibility of air, however incompressible hydraulics may be needed for high fidelity information transfer.

In this work, we propose a novel approach to improve astronaut dexterity without significantly increasing operational complexity, through passively actuated short-range tele-haptics (PAST). The proposed PAST approach includes an external hydraulically actuated mechanical hand attached to the arm of the user, connected to the user's hand and actuated via a linkage. The mechanical hand also houses a number of embedded hydraulic channels in the tip of each gripper finger, hydraulically connecting the fingertips of the external hand and the user's hand. The external mechanical hand enables the user's hand to be isolated from the real task, providing protection from hazards associated with EVA, while transferring haptic and tactile information.

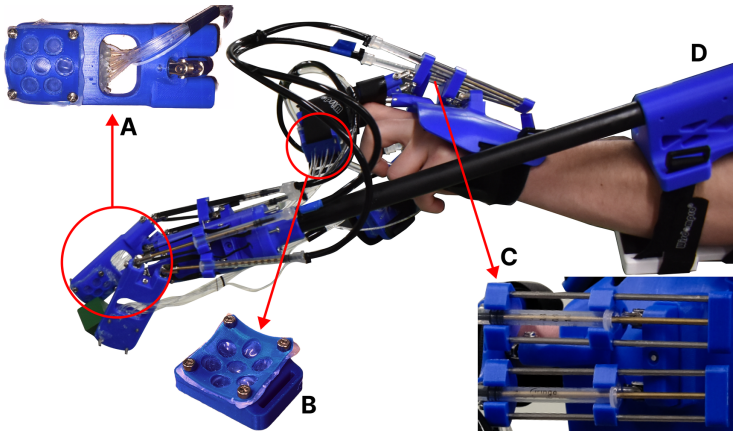

Figure 2 The PAST device being used to manipulate a small wooden block. The robot-side and human-side taxel arrays are visible in **A** and **B**, respectively. **C** shows the piston inversion mechanism, which enables the kinematically identical robot and human-side's hydraulic cylinders to have inversely proportional volumes, in order to result in a mimicking movement from the input and output. The robot arm is attached to the user's arm at **D**, and extended beyond the user's hand with a fiber-glass boom.

2 Design and Characterisation

2.1 Design Overview

The PAST device is designed to demonstrate simple manipulation and touch tasks and transmit the experience of tactile feedback. It is comprised of a human-facing hand interface and a robot hand which is mounted with an off-set on the users arm as seen in Fig. 2.

The PAST device has two principal subsystems: The haptic hydraulic linkage (HL), and the hydraulic taxel array (HTA). Both of these subsystems connect the human-facing hand interface and the attached robotic hand. Dexterous human manipulation relies on information

from the somatosensory system. Both shallow rapidly-adapting and deep slowly-adapting mechanoreceptors provide rate of skin indentation and depth of skin indentation information respectively [16]. The two subsystems provide input to stimulate both. Deep indentation from force feedback of grasping an object is provided by the HL, while the tactile information of specific position of contact, motion, and macro-scale texture are provided via the HTA.

This PAST prototype is designed to be manufactured with cheap and accessible materials, so as to allow rapid design iteration, and low-cost preliminary testing of the PAST concept. The HL uses proprietary $1ml$ syringes as hydraulic cylinders, and PVC tubing which are filled with silicone oil and connected to the syringes via a proprietary Luer lock secured with a zip-tie. Silicone oil was selected as the hydraulic fluid of the PAST device, due to its suitable thermal properties to withstand extreme hot and cold temperatures, and its prior use as a pressure distributor in MCP prototypes [20]. To ensure that the HL is rigid, the syringe plunger is replaced with a brass rod with a custom end-feature for securing the rubber plunger. The blue plastic components of the HL and HTA are 3D-printed, and secured with steel fasteners and superglue. The smaller $1mm$ internal diameter channels used for the HTA are also PVC, and secured in place first with guiding channels to push them into, and then with superglue and superglue accelerant to seal any gaps and secure them in place.

2.2 Haptic Hydraulic Linkage

The HL is designed to transfer the motion of the user's thumb and index finger to the robotic hand. The user's finger is constrained by a 2 degrees of freedom (2DoF) linkage that allows for flexion/extension and adduction/abduction motions. The motion of the finger determines the motion of two pistons, which hydraulically actuate two 'reversed syringes' on the robotic side. With the reversal of the syringes, the human-side and robot-side linkages are enabled to be kinematically identical as seen in Fig. 3.

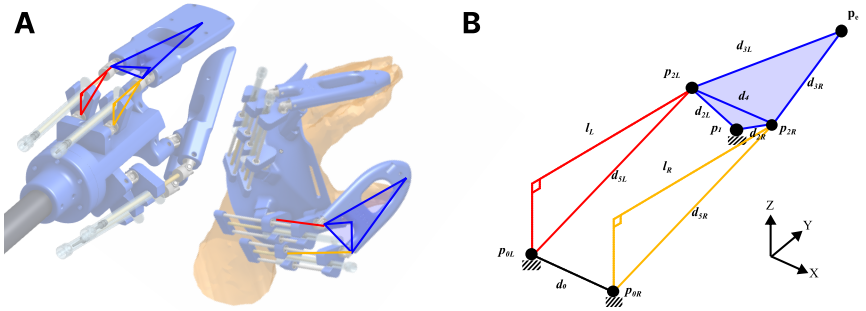

Figure 3 Image **A**: A kinematic diagram overlaid onto the design of the haptic hydraulic linkage (HL) gripper (left) and the HL hand interface (right) - illustrating their kinematic equivalence. Image **B**: The kinematic diagram of the HL, which is identical for both the human-facing and robotic side. The notation $\boldsymbol{p}_n$ denotes point vectors. Likewise, $\boldsymbol{d}_n$ denotes distance vectors which may change in direction but not magnitude, and $\boldsymbol{l}_n$ denotes the variable lengths of the pistons.

A two-fingered non-anthropomorphic design was chosen for the HL, allowing for the demonstration of grasping, while additional fingers would bring diminishing returns on what can be proven while increasing build complexity significantly. The thumb and index finger were chosen to be used, as they are the primary fingers used in manipulation. To mimic the relative position of the thumb and index finger, the two 2DoF fingers are offset at 135° relative to one another. The choice of two 2DoF fingers was done to mimic human-like pinch-grip

configurations, which rely on both the thumb and index being able to adduct/abduct. The possible relative configurations of two 2DoF fingers are very similar to having one 1Dof and one 2DoF finger, allowing the 2DoF finger to translate and rotate around the 1DoF. However, this would not reflect the way that the human manipulation with the thumb and index fingers is done.

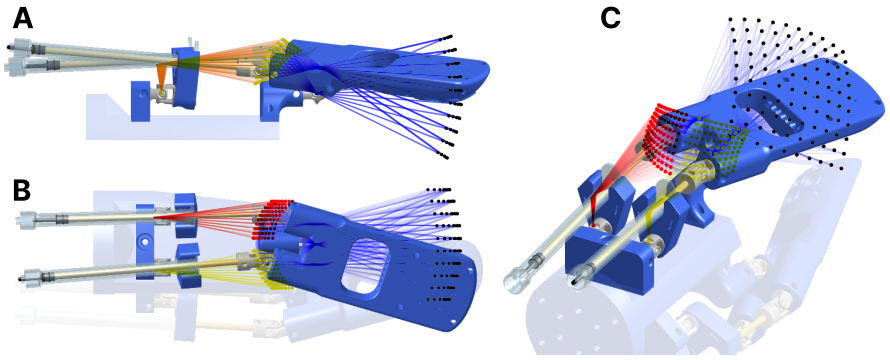

Figure 4 The kinematics can be used to generate a point-cloud of the workspace of an HL finger. The point-cloud and link positions are projected over an example position of the finger. **A** and **B** are orthogonal views, and **C** is an isometric view.

2.2.1 Forward Kinematics of the Robot Finger

The forward kinematics of the robot finger relate the length of each piston, $l_L^{(r)}$ and $l_R^{(r)}$ to the fingertip end-effector position $\boldsymbol{p}_e^{(r)}$ as seen in Fig. 3. Given that the finger is a rigid body, the rotation matrix $\mathrm{R}_e^{(r)}$ about the lower finger attachment joint is all that is necessary. We start by finding an expression for $\boldsymbol{p}_{2R}^{(r)}$, the position of the distal joint at the end of the right piston. $\boldsymbol{p}_{2R}^{(r)}$ lies on the intersection of two spheres: one centered on the proximal piston attachment point $\boldsymbol{p}_{0R}^{(r)}$ with radius defined by the vertical offset of the piston axis and the length of the piston $r_1^{(r)^2} = l_L^{(r)^2} + d_1^{(r)^2}$, and the other centered on the lower attachment point $\boldsymbol{p}_1^{(r)}$ with radius defined by a known initial offset $\boldsymbol{d}_{2R}^{(r)}$ such that $r_2^{(r)} = \left|\boldsymbol{d}_{2R}^{(r)}\right|$.

The intersection of two spheres is a circle with normal $\boldsymbol{n}_R^{(r)}$ pointing along the vector between the two centres of the spheres. The centre of the circle $\boldsymbol{c}_R^{(r)}$ is positioned along the vector between the sphere centres:

$$\boldsymbol{c}_R^{(r)} = \frac{\left|\boldsymbol{p}_1^{(r)} - \boldsymbol{p}_{0R}^{(r)}\right|^2 - r_2^{(r)^2} + r_1^{(r)^2}}{2\left|\boldsymbol{p}_1^{(r)} - \boldsymbol{p}_{0R}^{(r)}\right|} \cdot \boldsymbol{n}_R^{(r)}. \tag{1}$$

The radius of the circle $r_R^{(r)}$ can then be calculated:

$$r_R^{(r)^2} = r_1^{(r)^2} - \left|\boldsymbol{c}_R^{(r)}\right|^2, \tag{2}$$

and $\boldsymbol{p}_{2R}^{(r)}$ lies on this circle:

$$\left|\boldsymbol{p}_{2R}^{(r)} - \boldsymbol{c}_R^{(r)}\right|^2 = r_R^{(r)^2}. \tag{3}$$

Given that $\boldsymbol{p}_{2R}^{(r)}$ is equal to $\boldsymbol{p}_1^{(r)}$ plus the initial offset $\boldsymbol{d}_{2R}^{(r)}$ rotated around the lower attachment joint:

$$\boldsymbol{p}_{2R}^{(r)} = \mathrm{R}_e^{(r)} \boldsymbol{d}_{2R}^{(r)} + \boldsymbol{p}_1^{(r)}, \tag{4}$$

Which can also be written as a homogeneous transformation:

$$\boldsymbol{p}_{2R}^{(r)} = \begin{bmatrix} \mathrm{R}_e^{(r)} & \boldsymbol{p}_1^{(r)} \\ 0 & 1 \end{bmatrix} \boldsymbol{d}_{2R}^{(r)}, \tag{5}$$

an expression relating the rotation matrix $\mathrm{R}_e^{(r)}$ to the circle can be obtained:

$$\left| \mathrm{R}_e \boldsymbol{d}_{2R}^{(r)} + \boldsymbol{p}_1^{(r)} - \boldsymbol{c}_R^{(r)} \right|^2 = {r_R^{(r)}}^2. \tag{6}$$

Expanding and simplifying (6) yields:

$$2\left(\boldsymbol{p}_1^{(r)} - \boldsymbol{c}_R^{(r)}\right)^T \mathrm{R}_e^{(r)} \boldsymbol{d}_{2R}^{(r)} = {r_R^{(r)}}^2 - {r_2^{(r)}}^2 - \left| \boldsymbol{p}_1^{(r)} - \boldsymbol{c}_R^{(r)} \right|^2, \tag{7}$$

with an identical expression computed for the left-hand piston:

$$2\left(\boldsymbol{p}_1^{(r)} - \boldsymbol{c}_L^{(r)}\right)^T \mathrm{R}_e^{(r)} \boldsymbol{d}_{2L}^{(r)} = {r_L^{(r)}}^2 - {r_2^{(r)}}^2 - \left| \boldsymbol{p}_1^{(r)} - \boldsymbol{c}_L^{(r)} \right|^2. \tag{8}$$

Given that $\mathrm{R}_e^{(r)}$ is the compound of two rotations, and therefore there are only two unknown variables, equations (7) and (8) can be solved numerically to find the rotation of the finger about the lower attachment point.

2.2.2 Inverse Kinematics of the Human Finger

The inverse kinematics of the human finger relate the fingertip end-effector position $\boldsymbol{p}_e^{(h)}$ to the length of each piston, $l_L^{(h)}$ and $l_R^{(h)}$. Again, the finger is a rigid body, so the end-effector position determines the rotation of the finger about its lower attachment point $\mathrm{R}_e^{(h)}$:

$$\mathrm{R}_e^{(h)} \boldsymbol{d}_e^{(h)} + \boldsymbol{p}_1^{(h)} = \boldsymbol{p}_e^{(h)}, \tag{9}$$

Noting that $\mathrm{R}_e^{(h)}$ is comprised of sequential rotations about the z and x axes by θ_z and θ_x, respectively, (9) can be rewritten:

$$\mathrm{R}_{e,z}^{(h)}(\theta_z) \mathrm{R}_{e,x}^{(h)}(\theta_x) \boldsymbol{d}_e^{(h)} = \boldsymbol{p}_e^{(h)} - \boldsymbol{p}_1^{(h)}. \tag{10}$$

$\mathrm{R}_e^{(h)}$ takes the form:

$$\begin{bmatrix} c(\theta_z) & -s(\theta_z) & 0 \\ c(\theta_x)s(\theta_z) & c(\theta_x)c(\theta_z) & -s(\theta_x) \\ s(\theta_x)s(\theta_z) & s(\theta_x)c(\theta_z) & c(\theta_x) \end{bmatrix}, \tag{11}$$

where $c(\theta) = \cos(\theta)$ and $s(\theta) = \sin(\theta)$. The rotation about the z axis can be found by solving the x component of (10) for θ_z:

$$d_{e,x}^{(h)} c(\theta_z) - d_{e,y}^{(h)} s(\theta_z) = p_{e,x}^{(h)} - p_{1,x}^{(h)}. \tag{12}$$

Similarly, θ_x can be found by pre-multiplying (10) by $\mathrm{R}_e^{(h)T}$ and solving its z component for θ_x:

$$(p_{e,z}^{(h)} - p_{1,z}^{(h)})c(\theta_z) - (p_{e,y}^{(h)} - p_{1,y}^{(h)})s(\theta_z) = d_{e,z}^{(h)}. \tag{13}$$

There are four solutions to (12) and (13), from which the accepted solution can be chosen to maintain link length $|\boldsymbol{d}_e^{(h)}|$.

The location of the distal joint of the right piston can then be found from the rotation of the initial offset about the lower attachment point:

$$\boldsymbol{p}_{2R}^{(h)} = \mathrm{R}_e^{(h)}\boldsymbol{d}_{2R}^{(h)} + \boldsymbol{p}_1^{(h)}. \tag{14}$$

Knowing the positions of $\boldsymbol{p}_{0R}^{(h)}$ and $\boldsymbol{p}_{2R}^{(h)}$, and size of the perpendicular offset from the piston axis to its proximal attachment point $|\boldsymbol{d}_1^{(h)}|$, the length of the right piston $|\boldsymbol{l}_R^{(h)}|$ can be calculated:

$$|\boldsymbol{l}_R^{(h)}| = \sqrt{|\boldsymbol{p}_{2R}^{(h)} - \boldsymbol{p}_{0R}^{(h)}|^2 - |\boldsymbol{d}_1^{(h)}|^2}, \tag{15}$$

with an identical formulation for the left piston length $|\boldsymbol{l}_L^{(h)}|$.

2.2.3 Workspace

The workspace can be visualised by creating a point-cloud of end-effector positions computed via forward kinematics, as seen in Fig. 4. The dominant constraint of the workspace in practice is the range of motion permitted by the attached human finger, which will vary from user-to-user.

2.3 Hydraulic Taxel Array

The HTA transfers positional tactile information from the robotic hand to the finger-tips of the user. An HTA of 7 cells spaced 8 mm apart in a hexagonal grid is attached to each active finger via a finger interface, which is comprised of a fluid-filled channel with a molded silicone rubber bubble on both ends. These channels are routed through the plastic body of the robotic side to connect with thin 1.6 mm PVC tubing which in turn connects to the input points of the human-side finger interface as seen in Fig. 5. When the robotic-side bubble is deformed by applied pressure, it expands the human-side bubble, deforming the skin of the finger and transferring the feeling of touch. The user-side HTA is distributed around the fingertip, with the central taxel coinciding with the centre of the finger pad of the user.

The distance of 8 mm between the taxels was chosen firstly to simplify manufacturing of the prototype. However, this relatively large distance between each point approaches the limit of human two-point discrimination at the fingertip, which has been measured to be around $2 - 6$ mm [13].

2.3.1 Fabrication & Preparation

The taxel array was fabricated using a 'sandwich' structure, clamping a silicone membrane between the base-structure (the robot finger, or finger interface) and a 3D-printed plastic mesh as seen in Fig. 6. Once steel fasteners were in place to ensure that the silicone was under compression, superglue and adhesive accelerant were applied to the edges of the mesh and silicone structure, which sealed the edges, preventing leaks.

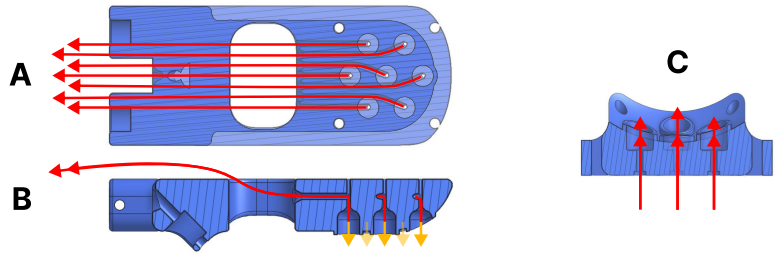

Figure 5 An illustration of the routing of hydraulic channels for the HTA. In **A** and **B** the channels of the robot side finger are shown, and how the pressure is transferred into the human side in image **C**. In **B** the narrow fill-points of each taxel which are designed for input with a needled syringe and easy sealing can be seen denoted by the yellow arrows.

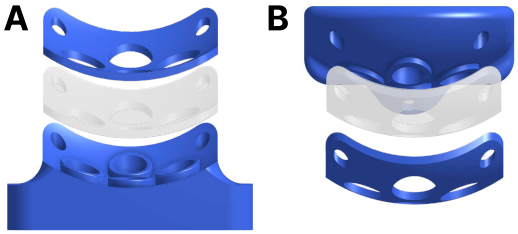

Figure 6 Image **A** and Image **B** show the taxel array fabrication, using a 'sandwich' structure of plastic and molded silicone rubber for the finger interface and robot finger, respectively. The curvature of the ergonomic finger interface is mirrored in the curvature of the robot finger. The holes on the corners of the clamping plastic mesh are to accommodate steel fasteners which allow for mechanical compression of the silicone layer, before sealing shut with adhesive.

In order to prepare the HTA, a narrow open channel for each taxel was included in the top of the robot-side finger, creating fill-points which can be accessed with a syringe and sealed with glue (denoted by yellow arrows in Fig. 5). This enables each taxel to be filled and sealed individually to the required initial pressure.

3 Performance Evaluation

3.1 Hydraulic Tactile Array Benchmarking

3.1.1 Positional Identification Methods

The identification of contact-points of the object being manipulated with the manipulator is an important factor of dexterous manipulation, and is the purpose of our somatosensory system [16]. In order to evaluate the tactility of the HTA against a heavy work glove (Fig. 7), 7 participants (1 female adult and 6 male adults) were asked to complete a blindfolded task of identifying which taxel or location on a heavy work glove (A, B, C, D, E, F, or G as in Fig. 9) was activated via a gentle depression with a soft rubber cylinder. The glove was selected as a benchmark due its tactile degradation being comparable to that of EVA glove [12]. The benchmark heavy work glove had an identical pattern to the taxel array marked onto it to ensure consistency in the relative positions of the pressure applications. To lighten the mental load for participants, a clock-face analogy was used to identify the 7 taxels, with [A, B, C, D, E, F, G] corresponding with [12'oclock, 10'oclock, 2'oclock, centre,

Figure 7 The benchmark heavy work glove with markings for input positions on the index finger (left), and the two-fingered human-side interface (right) used for testing the sensitivity to motion and positional pressure.

8'oclock, 4'oclock, and 6'oclock] (Fig. 8). In order to nullify the effects of learning in this study, participants were given the glove or taxel in a random order, in addition to the order of depressed location being randomised for both the glove and HTA.

3.1.2 Motion Direction Identification Methods

Sensing the motion of an object across the manipulating finger(s) is critical for robust dexterous manipulation [16]. In order to evaluate the performance of the HTA's ability to detect motion over the surface of the robotic finger, a blind-fold experiment was set up, and completed by 8 participants (7 male adults, 1 female adult), with each participant wearing the HTA and benchmark heavy work glove in turn. The participants were asked to turn a dial with their unencumbered hand, with the aim of matching the perceived direction of motion of an object as seen in Fig. 8. In order to nullify the effects of learning, participants were given the glove or the HTA in a random order. Each taxel/location was depressed 5 times in a randomised order, totalling 35 depressions per participant per trial.

4 Results & Discussion

4.1 Hydraulic Tactile Array Benchmarking

4.1.1 Positional Identification

The HTA improved fingertip positional information identification of users when compared to the baseline heavy work glove for all but one of the taxels (Fig. 9). A Mann-Whitney U test was performed to find whether the average accuracy was significantly improved for each taxel/position: A, E, and F had a p-value < 0.05, and that G's improvement had a p-value of < 0.01. This suggests that the direct contact of the silicone pads using the taxel array improves tactile sensitivity to direct pressure, especially around the lower fringes of the fingertip. Despite the low number of participants, the positive significance result for the taxels over the glove is promising for future applications of HTAs. Despite this, further experimentation is needed, due to the lack of explanation for the anomalously poor performance of the B taxel (10 o'clock) relative to the other taxels on the HTA, while a similar pattern is not observed in the glove's results. This may be explained by a manufacturing defect, or the positioning of the HTA on participants' fingers. The relationship between the

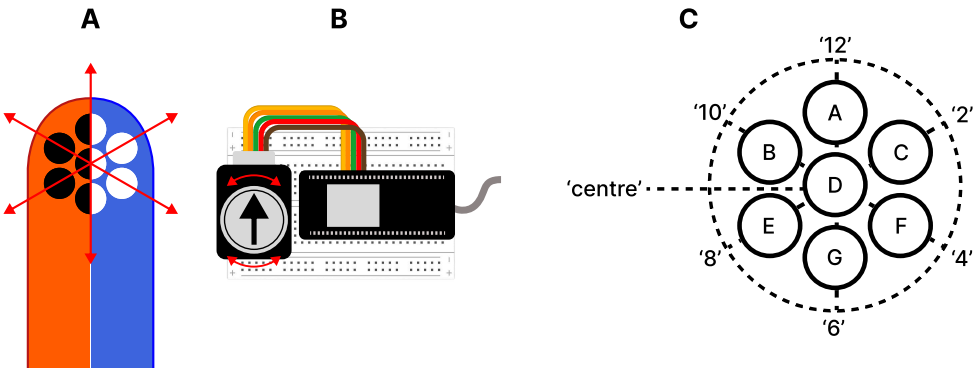

Figure 8 Illustrations of experiment methods. **A** represents the benchmark glove with markings and the HTA input. The red arrows denote the 6 directions in which the motion across the surface was applied during the motion direction experiments. **B** is a representation of the input device comprised of a dial and an STM-8266 based device used for the recording of the measured angle when the dial is depressed by the participant. **C** is the 'clock-face analogy' used to aid participants to report which location they felt pressure through the HTA or heavy work glove during the positional identification experiments. This enabled participants to visualise the input points in an easier way compared to the '$ABCDEFG$' format.

participants' finger-size and performance was investigated, as seen in Fig. 11. There is a positive correlation between finger size and performance on the positional accuracy tactility test with an R-squared of 0.67 for the HTA, and 0.34 for the glove. The equations for line of best fit for the HTA and glove results compared to participant finger size are:

$$y_h = 0.24x - 0.07, \ \& \ y_g = 0.29x - 0.45,$$

For the HTA, the gradient of its equation is shallower, suggesting that it may be less susceptible to tactile performance degradation with decreasing finger size (Fig. 11). However, without further investigation with a larger sample size, it is difficult to determine whether the difference between the two gradients is significant.

4.1.2 Motion Direction Identification

For the 8 participants who completed both the HTA and benchmark glove direction tests, the results showed that the mean absolute angular error between the perceived and real direction was decreased with the HTA but with low statistical significance per the Mann-Whitney U test, with significance levels for the 6 directions ranging between $p = 0.0849$ for 0°and $p = 0.9292$ for 120° . The significance of the improvement in the average performance among all directions as a single value is $p = 0.3095$.

The decreased significance of the performance improvement in the motion and direction test when compared to the positional stimuli test may be explained by the direction of strain in the fingertip, due to the anisotropic orientation and distribution of mechanoreceptors [3]. Interestingly, both the HTA and benchmark glove results exhibited anisotropic results, with the 300° direction being least accurate for both (Fig. 12). This could be due to the variance of sensitivity of the outer and inner edges of the index finger. This claim is supported by the asymmetrical mapping of mechanoreceptors on the finger-tip shown in Birznieks 2001 [3], but this hypothesis will need further testing to be validated.

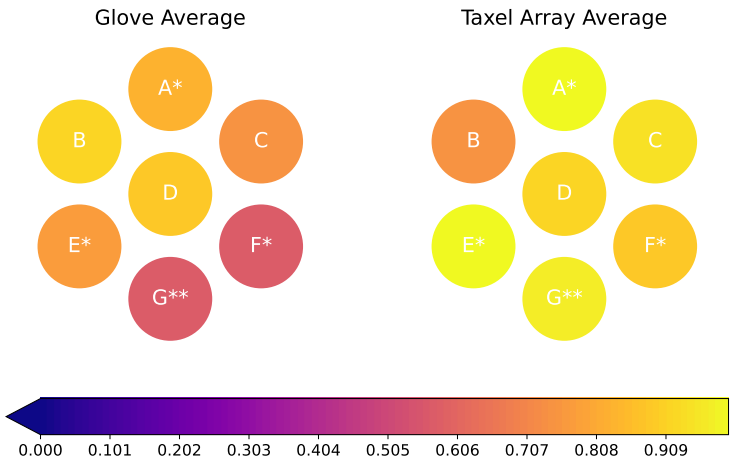

Figure 9 The average accuracy of identification of applied pressure for each location for the glove (left), and the taxel array (right). Statistical significance of the difference between the performance of the glove and taxel is calculated using a Mann-Whitney U test is shown as $* = p < 0.05$ and $** = p < 0.01$ level.

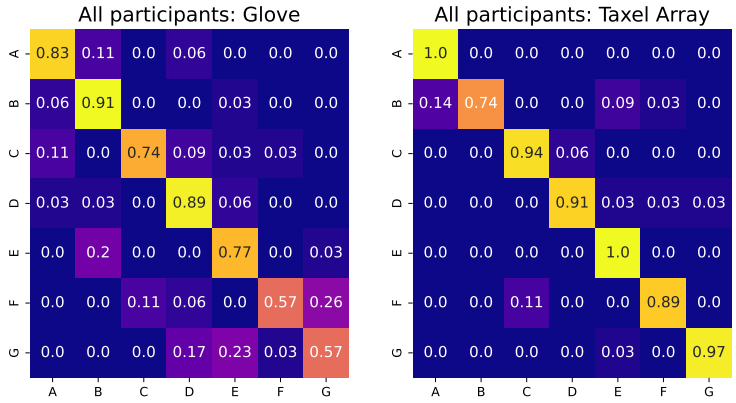

Figure 10 The confusion matrices showing the relationship between actual positional input vs perceived positional input for both the glove and the taxel array.

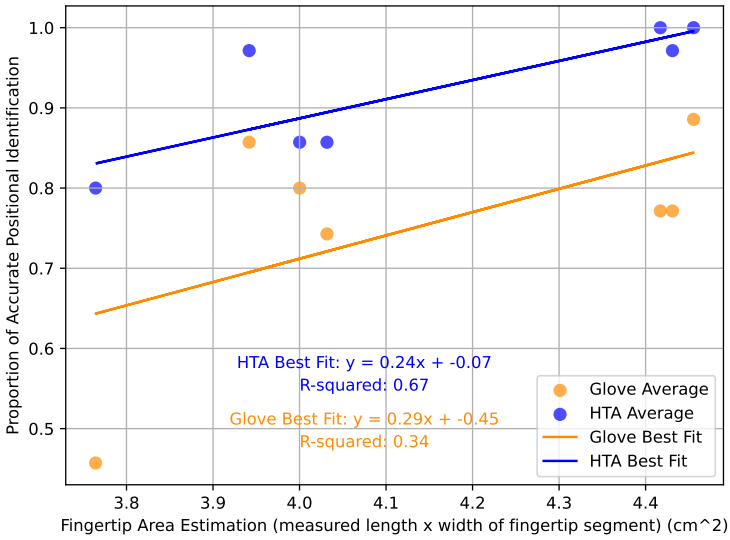

Figure 11 The relationship between a participant's finger area (calculated from measured finger segment length multiplied by the width), and their performance at the positional accuracy tactility test. There is a positive correlation between finger size and performance for both the HTA and glove.

4.2 Fabrication & Performance Discussion

The fabrication of the PAST device encountered several challenges, primarily related to sealing and bubble mitigation in both the Hydraulic Linkage (HL) and Hydraulically Actuated (HTA) subsystems. In the HL subsystem, the repeated use of proprietary syringes and Luer locks, originally designed for single-use, led to a degradation in their performance. While the choice of materials for the PAST device was suitable for proof-of-concept purposes, incorporating higher quality hydraulic cylinders would enhance the performance and longevity of future prototypes. The PVC tubing used for the transmission lines of the HL subsystem also introduced transparency issues due to diameter expansion under applied pressure. The effect of this in short tubes is minimal, but with additional length, the effect becomes substantial. This damping effect can be further exacerbated by the presence of air bubbles in the system, due to seal failure around the Luer locks and the syringe plunger. The effects of air in the lines is particularly noticeable when applying negative pressure through a transmission line with bubbles. This causes expansion of the air pockets, increasing the volume in the line, and if failing to overcome static friction, inhibiting movement of the end-effector. A possible solution to this issue is the bilateral pressurisation of hydraulic transmission lines by spring-loading both sides. However, this may not be necessary with the use of higher quality materials and seals, or with the implementation of a double-line approach, which ensures positive pressure in one of the lines in either direction, as is discussed in Whitney et al. as a comparison to their actuator [21].

Overall, overcoming challenges related to sealing and bubble mitigation is crucial to improving the fabrication and performance of the PAST device. The use of higher quality materials, improved seals, and the consideration of alternative pressurisation approaches can enhance the functionality and longevity of future prototypes.

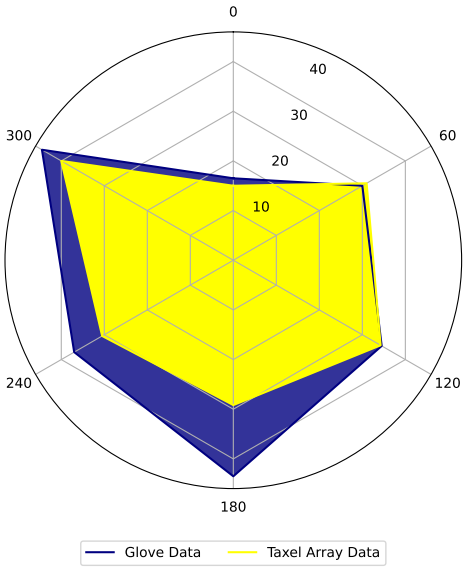

Figure 12 Mean absolute angular error of the participants using the heavy work glove and the taxel array (N=8) in the 6 motion input direction (0, 60, 120, 180, 240, and 300). The HTA results outperform the benchmark glove results, further investigation is needed to determine significance.

5 Conclusions

The PAST device has successfully demonstrated an alternative method for improving tactile sensitivity without compromising protection, offering a promising approach to enhance the dexterity of astronauts during EVA. However, further work is necessary to fully develop the PAST device paradigm for practical use.

5.1 Further Design Iterations

Improving the fidelity of prototypes by using higher-quality materials, actuators, and more complex HL designs, as well as integrating the PAST device with a pressurised protective suit, will bring PAST technology closer to the level required for practical applications.

Utilising a rolling seal for the HL cylinders such as is used in Whitney et. al. [21] and Lam et. al. [6] would not only increase the transparency of the mechanism but would also decrease static and *breakloose* friction by eliminating dry-contact area in the cylinders [8].

The main constraint of the PAST device's utility is the design of the robotic hand. The two 2DoF fingered design cannot perform important actions that the human hand is capable of, such as prehensile grips, form-clasping, and caging. To address some of these issues, the design can be updated in a number of ways:

- An alternative linkage design can be developed for the HL, which may enable form-clasping, such as the 2DoF per finger design used by the thumb and index of the Festo ExoHand to both track and actuate motion [5].
- The addition of more fingers to the HL would enable complex in-hand manipulation, such as in the RUTH hand [9].
- The addition of additional transferable degrees of freedom from the human-side to the robot-side of the HL. This would enable more natural and complex movements to be transmitted, increasing anthropomorphism.

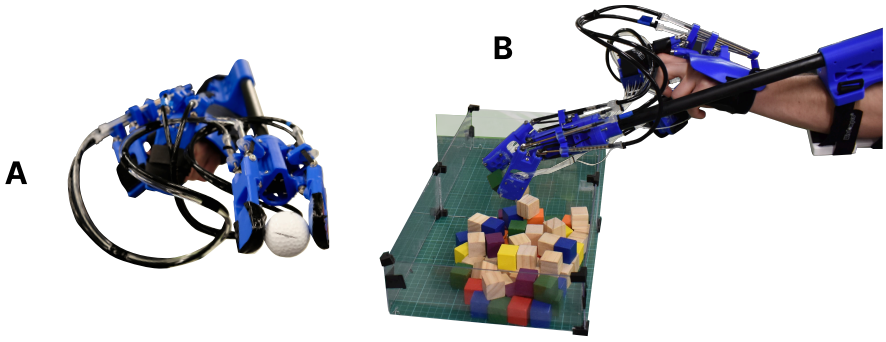

Figure 13 **A** shows the HL without the HTA picking up and manipulating a golf ball. **B** shows a block manipulation demonstration task being carried out with the HL and HTA subsystems combined.

The PAST device successfully transfers tactility, but with an extended limb, a perception of *embodiment* can be expected with the robotic hand [4]. However, further work must be done to validate embodiment.

5.2 Alternative applications

Beyond use for improving dexterity in space, PAST devices have further applications in environments and situations which favour a layer of separation between the operator and the task, while relying on local communication. These applications could include use by deep-sea divers, HazMat handlers, and even actors wearing decorative exo-suits as an attraction at theme-parks. The principles of PAST could also be applied in the precise control of machinery or tools, such as emergency surgery with surgical robots that require no external power.

5.3 Final Comment

In conclusion, the PAST approach shows promise in enhancing astronaut dexterity during EVA as well as other potential applications. Preliminary data indicates significant improvement in positional tactile sensitivity and some improvement in directional tactile sensitivity when compared to HWGs. However, further investigation is needed for comparison with high-fidelity pressurised EVA gloves. The tactility experiments have also revealed insights into the varying sensitivity of the fingertip, prompting further research questions in this area. Initial grasp and manipulation abilities have been demonstrated, but further experimentation is required to fully characterise the prototype. Overall, the preliminary tests provide a clear direction for further iteration and development of passively actuated short-range telehaptic devices.

References

1 Ryan Z. Amick, Christopher R. Reid, Linh Q. Vu, Dan Nguyen, Robert Sweet, Shane McFarland, and Sudhakar Rajulu. Preliminary assessment of ergonomic injury risk factors in the extravehicular mobility unit spacesuit glove. In *Proceedings of the Human Factors and Ergonomics Society*, pages 981–985. Human Factors an Ergonomics Society Inc., 2016. doi:10.1177/1541931213601227.

2 Christian Antfolk, Anders Björkman, Sven Olof Frank, Fredrik Sebelius, Göran Lundborg, and Birgitta Rosen. Sensory feedback from a prosthetic hand based on air-mediated pressure from the hand to the forearm skin. *Journal of rehabilitation medicine*, 44:702–707, 2012. doi:10.2340/16501977-1001.

3 Ingvars Birznieks, Per Jenmalm, Antony W. Goodwin, and Roland S. Johansson. Encoding of direction of fingertip forces by human tactile afferents. *Journal of Neuroscience*, 21:8222–8237, October 2001. doi:10.1523/JNEUROSCI.21-20-08222.2001.

4 H. Henrik Ehrsson, Charles Spence, and Richard E. Passingham. That's my hand! activity in premotor cortex reflects feeling of ownership of a limb. *Science*, 305:875–877, August 2004. doi:10.1126/science.1097011.

5 Festo. Exohand | festo usa, 2012. URL: https://www.festo.com/us/en/e/about-festo/research-and-development/bionic-learning-network/highlights-from-2010-to-2012/exohand-id_33631/.

6 Hoi Man Lam, W Jared Walker, Lucas Jonasch, Dimitri Schreiber, and Michael C Yip. Design and mechanics of cable-driven rolling diaphragm transmission for high-transparency robotic motion. In *2023 IEEE International Conference on Robotics and Automation (ICRA)*, pages 7338–7344. IEEE, 2023. doi:10.1109/ICRA48891.2023.10160832.

7 Dan F. Lester, Kip V. Hodges, and Robert C. Anderson. Exploration telepresence: A strategy for optimizing scientific research at remote space destinations. *Science Robotics*, 2:4383, June 2017. doi:10.1126/SCIROBOTICS.AAN4383.

8 B. Lorenz, B. A. Krick, N. Rodriguez, W. G. Sawyer, P. Mangiagalli, and B. N.J. Persson. Static or breakloose friction for lubricated contacts: the role of surface roughness and dewetting. *Journal of physics. Condensed matter : an Institute of Physics journal*, 25, November 2013. doi:10.1088/0953-8984/25/44/445013.

9 Qiujie Lu, Nicholas Baron, Angus B. Clark, and Nicolas Rojas. Systematic object-invariant in-hand manipulation via reconfigurable underactuation: Introducing the ruth gripper. *International Journal of Robotics Research*, 40:1402–1418, December 2021. doi:10.1177/02783649211048929.

10 Shane M Mcfarland, Amy J Ross, and Robert W Sanders. The "space activity suit" – a historical perspective and a primer on the physiology of mechanical counter-pressure. In *International Conference on Environmental Systems*. 49th International Conference on Environmental Systems, July 2019. URL: https://ttu-ir.tdl.org/handle/2346/84941.

11 M Mehdi, S Mousavi, Elisa Paola Ambrosio, Silvia Appendino, Fai Chen Chen, Alain Favetto, Diego Manfredi, Francesco Pescarmona, and Aurelio Somà. Spacesuits and eva gloves evolution and future trends of extravehicular activity gloves. Technical report, American Institute of Aeronautics and Astronautics, 2011.

12 NASA. Man-system integration standards section 14 - extravehicular activity. Technical report, NASA, 1995. URL: https://msis.jsc.nasa.gov/default.htm.

13 Julie Rowin and Matthew N. Meriggioli. Proprioception, touch, and vibratory sensation. *Textbook of Clinical Neurology: Third Edition*, pages 343–361, January 2007. doi:10.1016/B978-141603618-0.10019-0.

14 Thomas B. Sheridan. Space teleoperation through time delay: Review and prognosis. *IEEE Transactions on Robotics and Automation*, 9:592–606, 1993. doi:10.1109/70.258052.

15 Bobby L. Shields, John A. Main, Steven W. Peterson, and Alvin M. Strauss. An anthropomorphic hand exoskeleton to prevent astronaut hand fatigue during extravehicular activities. *IEEE Transactions on Systems, Man, and Cybernetics Part A:Systems and Humans.*, 27:668–673, 1997. doi:10.1109/3468.618265.

16 Anton R. Sobinov and Sliman J. Bensmaia. The neural mechanisms of manual dexterity. *Nature Reviews Neuroscience*, 22:741–757, December 2021. doi:10.1038/s41583-021-00528-7.

17 Theodore C Southern and Nikolay A Moiseev. Novel mechanical counter pressure gloves. In *International Conference on Environmental Systems*, 2017. URL: https://ttu-ir.tdl.org/bitstream/handle/2346/72920/ICES_2017_97.pdf?sequence=1&isAllowed=y.

18 Russell H. Taylor and Dan Stoianovici. Medical robotics in computer-integrated surgery. *IEEE Transactions on Robotics and Automation*, 19:765–781, October 2003. doi:10.1109/TRA.2003.817058.

19 Yinsheng Tian, Haibo Zhang, Li Wang, Li Ding, and Deyu Li. Effects of eva glove on hand dexterity at low temperature and low pressure. *Applied Ergonomics*, 70:98–103, July 2018. doi:10.1016/j.apergo.2018.02.008.

20 Pad Webb and James F Annis. Nasa - the principle of the space activity suit. Technical report, NASA, 1967.

21 John P Whitney, Tianyao Chen, John Mars, and Jessica K Hodgins. A hybrid hydrostatic transmission and human-safe haptic telepresence robot. *IEEE International Conference on Robotics and Automation (ICRA)*, 2016. doi:10.1109/ICRA.2016.7487195.